Published OnlineFirst October 4, 2018; DOI: 10.1158/1078-0432.CCR-18-1941

Translational Cancer Mechanisms and Therapy

Clinical Cancer Research

Clinical Significance of Extracellular Vesicles in Plasma from Glioblastoma Patients

Daniela Osti[1], Massimiliano Del Bene[1,2], Germana Rappa[3], Mark Santos[3], Vittoria Matafora[4], Cristina Richichi[1], Stefania Faletti[1], Galina V. Beznoussenko[4], Alexandre Mironov[4], Angela Bachi[4], Lorenzo Fornasari[1], Daniele Bongetta[5,6], Paolo Gaetani[5], Francesco DiMeco[2,7,8], Aurelio Lorico[3,9], and Giuliana Pelicci[1,10]

Abstract

Purpose: Glioblastoma (GBM) is the most common primary brain tumor. The identification of blood biomarkers reflecting the tumor status represents a major unmet need for optimal clinical management of patients with GBM. Their high number in body fluids, their stability, and the presence of many tumor-associated proteins and RNAs make extracellular vesicles potentially optimal biomarkers. Here, we investigated the potential role of plasma extracellular vesicles from patients with GBM for diagnosis and follow-up after treatment and as a prognostic tool.

Experimental Design: Plasma from healthy controls ($n = 33$), patients with GBM ($n = 43$), and patients with different central nervous system malignancies ($n = 25$) were collected. Extracellular vesicles were isolated by ultracentrifugation and characterized in terms of morphology by transmission electron microscopy, concentration, and size by nanoparticle tracking analysis, and protein composition by mass spectrometry. An orthotopic mouse model of human GBM confirmed human plasma extracellular vesicle quantifications. Associations between plasma extracellular vesicle concentration and clinicopathologic features of patients with GBM were analyzed. All statistical tests were two-sided.

Results: GBM releases heterogeneous extracellular vesicles detectable in plasma. Plasma extracellular vesicle concentration was higher in GBM compared with healthy controls ($P < 0.001$), brain metastases ($P < 0.001$), and extra-axial brain tumors ($P < 0.001$). After surgery, a significant drop in plasma extracellular vesicle concentration was measured ($P < 0.001$). Plasma extracellular vesicle concentration was also increased in GBM-bearing mice ($P < 0.001$). Proteomic profiling revealed a GBM-distinctive signature.

Conclusions: Higher extracellular vesicle plasma levels may assist in GBM clinical diagnosis: their reduction after GBM resection, their rise at recurrence, and their protein cargo might provide indications about tumor, therapy response, and monitoring.

Introduction

Glioblastoma (GBM) is the most common primitive tumor of the central nervous system (CNS), accounting for 12%–15% of all intracranial tumors (1). Actual standard of care is based on maximal surgical resection followed by chemotherapy and radiotherapy (1, 2). Despite many efforts to find new therapeutic approaches, GBM patients' median overall survival (OS) is 14 months from diagnosis (1, 2). Diagnosis and follow-up are usually feasible with imaging techniques after tumor becomes clinically evident. Molecular characterization of GBM for classification, grading, and inclusion of patients in clinical trials is possible only with specimens obtained with open surgery or biopsy. In this context, extracellular vesicles could play an important role both for research and clinical purposes. Extracellular vesicles are small structures (50–1,000 nm) surrounded by a lipid membrane bilayer, released in the extracellular space from normal and neoplastic cells (3–5). Extracellular vesicles include exosomes (50–150 nm, originating from the endosomal pathway) and microvesicles (up to 1,000 nm, shed from the plasma membrane). Their cargo encompasses proteins, RNA, and lipids specific for the cell of origin (3–5). In the neoplastic setting, they induce tumor progression and infiltration, sustain neoangiogenesis, inhibit immune response, and lead to chemo/radio-resistance (3, 6–12). Interestingly, extracellular vesicles can be used as circulating biomarkers because they can be easily isolated from bloodstream, urine, cerebrospinal, ascitic, amniotic, and seminal fluid (4). An increasing number of studies have addressed the use of extracellular vesicles as cancer biomarkers relying on their cargo (13, 14). In addition, circulating extracellular vesicles support the

[1]Department of Experimental Oncology, IEO, European Institute of Oncology IRCCS, Milan, Italy. [2]Department of Neurosurgery, Fondazione IRCCS Istituto Neurologico Carlo Besta, Milan, Italy. [3]College of Medicine, Roseman University of Health Sciences, Las Vegas, Nevada. [4]IFOM, the FIRC Institute of Molecular Oncology, Milan, Italy. [5]Neurosurgery Unit, IRCCS Fondazione Policlinico San Matteo, Pavia, Italy. [6]Department of Clinical-Surgical, Diagnostic and Paediatric Sciences, Università degli Studi di Pavia, Pavia, Italy. [7]Department of Neurological Surgery, Johns Hopkins Medical School, Baltimore, Maryland. [8]Department of Pathophysiology and Transplantation, University of Milan, Milan, Italy. [9]Mediterranean Institute of Oncology Foundation, Viagrande, Italy. [10]Department of Translational Medicine, Piemonte Orientale University "Amedeo Avogadro," Novara, Italy.

Note: Supplementary data for this article are available at Clinical Cancer Research Online (http://clincancerres.aacrjournals.org/).

D. Osti, M. Del Bene, and G. Rappa contributed equally to this article.

A. Lorico, and G. Pelicci are senior authors for their specific research fields.

Corresponding Author: Giuliana Pelicci, European Institute of Oncology, Milan 20139, Italy. Phone: 3902-5748-9830; Fax: 3902-9437-5990; E-mail: giuliana.pelicci@ieo.it

doi: 10.1158/1078-0432.CCR-18-1941

©2018 American Association for Cancer Research.

Downloaded from clincancerres.aacrjournals.org on January 27, 2021. © 2019 American Association for Cancer Research.

Published OnlineFirst October 4, 2018; DOI: 10.1158/1078-0432.CCR-18-1941

Translational Relevance

Glioblastoma (GBM) represents one of the most aggressive and therapeutically challenging cancers due to its growth and infiltration ability throughout the brain. GBM treatment aims to detect the tumor at an early stage and to follow its progression. The results of this study support the possibility to diagnose GBM and to follow its response to therapy through a minimally invasive blood sample. This would be of remarkable value for the patient by facilitating clinical decision-making without the need for imaging. Furthermore, we characterized the protein cargo of plasma GBM extracellular vesicles detecting a specific GBM signature which could be suitable to detect tumor, to characterize its molecular profile and, potentially, to tailor treatment in accordance to each patient's case. We could expect that our results, taking advantage from currently emerging technologies for fast extracellular vesicle purification and characterization, will lead to a rapid translation in routine clinical practice.

possibility to detect intraepithelial lesions in very early stages, not yet discernible by MRI (15). A direct relationship between exosome levels and tumor burden, recurrence, and OS of patients with cancer has been observed (14, 15). Moreover, analysis of exosomal molecular cargo, specifically profiling of proteins or RNA, has potential clinical value (14). Likewise, extracellular vesicles released by GBMs into peripheral blood could be used as clinical biomarkers (9, 14, 16–18).

Here, we characterized extracellular vesicles isolated from plasma of patients with GBM for morphology, size, concentration, and protein profile to validate the role of GBM-derived extracellular vesicles as specific biomarkers for early diagnosis, follow-up after treatment, and as prognostic tool. We correlated the characteristics of extracellular vesicles isolated from plasma of patients with GBM before and after surgery with those of healthy controls and of patients harboring other CNS malignancies. Moreover, we employed patient-derived xenograft (PDX) model to confirm the specificity of extracellular vesicle features observed in patients with GBM.

Materials and Methods

Patients and clinical samples

Healthy individuals ($n = 33$) and consenting patients with GBM ($n = 43$) or other CNS malignancies ($n = 25$) were enrolled at the Department of Neurosurgery of "C. Besta" Neurological Institute (Milan, Italy) and at the Department of Neurosurgery of San Matteo Hospital (Pavia, Italy) upon approval from the research ethics committee and in accordance with the ethical guidelines outlined in the Declaration of Helsinki. The healthy controls were blood donors matched for age and sex. Patients with GBM were consistent with other published clinical series concerning age, sex distribution, dimensional range, Karnofsky performance status scale, necrosis, presentation symptoms, tumor site, IHC staining, postsurgical treatment, PFS, and OS (19). Tumor necrosis was graded in T1 plus gadolinium weighted MRI as follow: (i) necrosis volume < 1/3 of total tumor volume; (ii) necrosis volume > 1/3 and < 2/3 of total tumor volume; and (iii) necrosis volume > 2/3 of total tumor volume. Tumor size was measured in axial T1 plus gadolinium weighted MRI as the maximum diameter of the contrast-enhancing mass. IHC staining was aimed at identifying EGFR expression/amplification [EGFR Ab-10 (clone 111.6), 2 μg/mL, mouse mAB, Thermo Fisher Scientific], MGMT expression [anti-MGMT (clone MT 3.1), 1:100, mouse mAB, Millipore], PTEN deletion [sc-7974 (A2B1), 1:100, mouse mAB, Santa Cruz Biotechnology], P53 mutation [anti-Human p53 protein (clone DO-7), 1:50, mouse mAB, Merck KGaA], IDH1 mutation [anti-human IDh1 R132H, (clone H09), 1:50, mouse mAB, Dianova GmbH]. Regarding the detection of P53 mutation, we exploited the different stability of wild-type versus mutant p53 protein. Wild-type p53 is relatively unstable and characterized by a very short half-life, which makes it undetectable by IHC. On the contrary, mutant p53 has a much longer half-life, accumulates in the nucleus, and become therefore detectable (20).

OS and PFS have been measured as elapsed time from surgery to death or to the diagnosis of recurrence/ progression in accordance to RANO criteria (21). Details of patients with GBM are summarized in Supplementary Tables S1 and S2.

Human plasma collection and extracellular vesicle isolation

Blood samples were collected at diagnosis (before the operation; baseline) or 3 days after surgery for postoperative GBM samples. Peripheral blood (15 mL) was collected in tubes containing disodium EDTA (Sarstedt) and processed to obtain plasma through centrifugation at $2,000 \times g$ for 15 minutes at 4°C not later than 4 hours after withdrawal. The collected plasma samples were then pelleted by differential centrifugation (22). Briefly, they were centrifuged at $12,000 \times g$ for 30 minutes at 4°C, ultrafiltered using a 0.22-μm filter (EMD Millipore), and ultracentrifuged at $110,000 \times g$ for 2 hours at 4°C. Extracellular vesicle pellet was washed once in PBS and ultracentrifuged at $110,000 \times g$ for 2 hours at 4°C. The pelleted extracellular vesicles were resuspended in PBS and kept at −80°C.

Electron microscopy

Tissue block preparation, electron microscopy (EM) examination, and immune EM analysis were performed as described previously (23–25), with modifications. A description of each process is given.

Embedding. Purified extracellular vesicles and the brain tissue were fixed with of 4% paraformaldehyde (PFA) and 2.5% glutaraldehyde (EMS) mixture in 0.2 mol/L sodium cacodylate (pH 7.2) for 2 hours at room temperature, followed by 6 washes in 0.2 mol/L sodium cacodylate (pH 7.2) at room temperature. Samples were incubated in 1:1 mixture of 2% osmium tetraoxide and 3% potassium ferrocyanide for 1 hour at room temperature followed by 6 times rinsing in 0.2 mol/L cacodylate buffer. They were sequentially treated with 0.3% thiocarbohydrazide in 0.2 mol/L cacodylate buffer for 10 minutes and 1% OsO4 in 0.2 mol/L cacodylate buffer (pH 6.9) for 30 minutes, then rinsed with 0.1 mol/L sodium cacodylate (pH 6.9) buffer until all traces of the yellow osmium fixative have been removed, washed in deionized water, treated with 1% uranyl acetate in water for 1 hour, and washed in water again (24, 26). The samples were subsequently subjected to dehydration in ethanol and then in acetone, and embedded in Epoxy resin at room temperature and polymerized for at least 72 hours in a 60 °C oven. Embedded samples were then

Downloaded from clincancerres.aacrjournals.org on January 27, 2021. © 2019 American Association for Cancer Research.

Published OnlineFirst October 4, 2018; DOI: 10.1158/1078-0432.CCR-18-1941

sectioned with Diamond Knife (Diatome) using Leica ultramicrotome. Sections were analyzed with a Tecnai 20 High Voltage EM (FEI, Thermo Fisher Scientific) operating at 200 kV (26).

Electron tomography. An Ultramicrotome (Leica EM UC7) was used to cut 60-nm serial thin sections and 200-nm serial semithick sections. Sections were collected onto 1% formvar films adhered to slot grids. Both sides of the grids were labeled with fiduciary 10-nm gold (PAG10). Tilt series were collected from the samples from ± 65° with 1° increments at 200 kV in Tecnai 20 Electron Microscopes (FEI, Thermo Fisher Scientific). Tilt series were recorded at a magnification of 11,500 ×, 14,500 ×, 19,000 ×, or 29,000 × using software supplied with the instrument. The nominal resolution in our tomograms was 4 nm, based on section thickness, the number of tilts, tilt increments, and tilt angle range. The IMOD 4.0.11 package was used to construct individual tomograms and for the assignment of the outer leaflet of organelle membrane contours and best-fit sphere models of the outer leaflet were used for vesicle measurements.

Ultrathin cryosectioning and labeling of cryosections. Extracellular vesicles were fixed by adding of a mixture of 0.1 mol/L PHEM buffer, 2% PFA, and 1% glutaraldehyde for 2 hours, and finally stored in storage solution (0.1 mol/L PHEM buffer and 0.5% PFA in distilled water) overnight. After washing with 0.15 mol/L glycine buffer in PBS, extracellular vesicles were embedded in 12% gelatin, cooled on ice, and cut into 0.5-mm blocks in the cold room. The blocks were infused with 2.3 mol/L sucrose, which acts as a cryoprotectant, and then placed onto small specimen pins. Pins were frozen by immersion in liquid nitrogen, quickly transferred to a precooled (−60 °C) cryo-chamber fitted onto an Ultramicrotome (Leica EM UC7) and trimmed to a suitable shape. The sections were cut at −120 °C using a dry diamond knife and collected on the knife surface. Sections were retrieved from the knife by picking them up on a small drop of a 1:1 mixture of 2.3 mol/L sucrose and 2% methyl cellulose and transferred onto formvar- and carbon-coated specimen grids. Samples were then processed for immune-labeling. Grids were kept floating on drops of buffered saline solution with the section side in the liquid. The back of the grid was kept dry and the section side was kept hydrated at all times. The grids were washed onto 100-μL droplets of PBS for 10 minutes and then additionally washed 3 × 3 minutes with 0.02 mol/L glycine in PBS, pH 7.4. The grids were incubated for 10 minutes in 0.5% BSA- cTM in PBS (BSA-cTM, acetylated BSA, 10% in water) and then incubated for 2 hours on 10-μL droplets of CD9 primary antibody (1:10, mouse mAB, BD Pharmigen). The grids were washed 6 times with 0.1 % BSA-cTM in PBS. Next, we used a rabbit anti-mouse immunoglobulin antibody (bridge antibody, 1:250, Dako) and then with protein-A gold 10 nm (PAG10) 1:50 diluted in blocking solution for 20 minutes at room temperature. The grids were rinsed 6 times with 0.1% BSA-cTM in PBS and postfixed with 1% glutaraldehyde in 0.15 mol/L HEPES for 5 minutes. Finally, the grids were washed 5 × 1 minute in distilled water and stained for 10 minutes in 1.8% methyl cellulose plus 0.4% uranyl acetate on ice. The grids were retrieved with a stainless steel loop onto a piece of a Whatman 50 filter paper at an angle of 45°. After air-drying, the grids were examined under Tecnai20 Electron Microscope (FEI, Thermo Fisher Scientific).

Nanoparticle tracking analysis

Extracellular vesicle samples diluted in PBS were analyzed using a LM10 nanoparticle tracking analyzer with 532-nm laser (Malvern Panalytical; ref. 27). Briefly, extracellular vesicles in PBS were analyzed using a LM10 nanoparticle tracking analyzer with 532-nm laser (Malvern Panalytical). Six videos of 30 seconds were recorded for each sample and analyzed under constant settings to obtain data on mean particle size, size distribution, and particle concentration. Because nanoparticle tracking analysis (NTA) is most accurate between particle concentrations in the range of 2 × 108 to 2 × 109/mL, when samples contained higher numbers of particles, they were diluted before analysis and the relative concentration calculated according to the dilution factor.

Lentiviral-mediated CD9 overexpression in GBM tumor-initiating cells

GBM tumor-initiating cells (TIC) were transduced with prepackaged CD9-GFP virus (pCT-CD9-GFP, CYTO122-VA-1; System Biosciences SBI). Seventy-two hours after infection, transduced cells were FACS-sorted (FACS Aria, Becton Dickinson) to separate GFP-positive (GFP^+) from GFP-negative (GFP^-) fractions. Cell sorting was performed at room temperature with the laser (Coherent Innova 70) set at 488 nm wavelength and 100 mW power. Forward scatter (FSC) and side scatter (SSC) were collected through a filter. The EGFP signal was collected in the FL1 channel through a 530/40 bandpass filter. A light scatter gate was drawn in the SSC versus FSC plot to exclude debris. Cells in the gate were displayed in a single-parameter histogram for the EGFP and final gating settings determined to collect the labeled cells.

In vivo assay

For quantification of GBM-derived extracellular vesicles, TICs isolated from human GBM tissues (10^5 cells in 2-μL PBS) were stereotaxically injected into the nucleus caudatus (1-mm posterior; 3-mm left lateral; and 3.5 mm in depth from bregma) of 5 weeks-old female nu/nu CD-1 mice (Charles River; ref. 28). Seven days later, mice were sacrificed and brains and plasma were harvested. Plasma was also harvested from nontransplanted mice. Plasma extracellular vesicles were isolated as hereinafter described and quantified by NTA. These experiments were performed two times, using 5 animals per group.

In vivo experiments were approved by the Institute Ethical Committee for animal use and conducted in accordance with the Italian Ministry of Health (D.L.vo 116/92 and following additions).

Confocal laser scanning microscopy

Plasma extracellular vesicles from nontransplanted mice or mice harboring intracranial human GFP^+ GBMs were stained with 5 μmol/L of the membrane dye 1,1′-dioctadecyl-3,3,3′,3′-tetramethylindocarbocyanine perchlorate (Dil; Thermo Fisher Scientific) for 20 minutes at 37°C. To remove excess dye, the extracellular vesicles were transferred into a spin column (Exosome Spin Columns, MW 3000, Thermo Fisher Scientific) and centrifuged at 750 × *g* for 2 minutes. The process was repeated twice. DiI-labeled extracellular vesicles in PBS were then placed in 35-mm glass-bottom dishes coated with poly-D-lysine (MatTek Corporation) for 30 minutes before being analyzed by confocal laser-scanning microscopy (CLSM) using a Nikon A1R+ inverted

Downloaded from clincancerres.aacrjournals.org on January 27, 2021. © 2019 American Association for Cancer Research.

Published OnlineFirst October 4, 2018; DOI: 10.1158/1078-0432.CCR-18-1941

confocal microscope with a 60X Apo-TIRF oil-immersion objective and a numerical aperture of 1.49 at 1024 × 1024 pixel resolution. 488 and 561 solid-state lasers were used to excite GFP and DiI, respectively, and corresponding fluorescence emissions were collected using 500–550 and 570–620-nm long-pass filters. All images were acquired under the same microscope settings and recorded using NIS Elements Software (Nikon).

IHC

Xenografted mouse brains were formalin-fixed, paraffin-embedded according to established procedures. Tissue sections (3 μm) were incubated with the following primary antibodies: anti-nuclei (mouse mAB, 1:1,000, clone 3E1.3, Millipore) and anti-GFP (rabbit polyclonal antibody, 1:1,000, sc8334, Santa Cruz Biotechnology). All sections were counterstained with Mayer hematoxylin and visualized using a bright-field microscope.

Western immunoblotting

Plasma extracellular vesicles were solubilized in 8 mol/L urea, 0.1 mol/L Tris/HCl, pH 8.5. Extracellular vesicle protein concentrations were assessed by Bradford Assay (Bio-Rad) and extracellular vesicle lysates (10 μg) were analyzed by standard Western immunoblotting. Briefly, extracellular vesicle lysates were loaded onto a SDS-PAGE under reducing conditions, and resolved proteins were transferred on to Nitrocellulose Transferring Membranes (Protran) of 0.2-μm pore size. After blocking with 5% nonfat dry milk in Tris-buffered saline and Tween 20 [TBS-T (50 mmol/L Tris, 150 mmol/L NaCl, and 0.05% Tween 20)], membranes were incubated overnight at 4°C with the primary antibodies CD63 [sc-15363 (H-193), 1:100, rabbit polyclonal antibody, Santa Cruz Biotechnology], tsg101 [sc-6037 (M-19), 1:500, goat polyclonal antibody, Santa Cruz Biotechnology], and CD9 (1:500, mouse mAB, BD Pharmigen). Antibody binding was assessed by horseradish peroxidase–conjugated secondary antibody (1:10,000, Sigma Aldrich). Immunoreactive bands were detected with ECL Western Blotting Reagents (GE Healthcare Bio-Sciences).

Proteomic analysis

Extracellular vesicle pellets were solubilized in 8 mol/L urea, 0.1 mol/L Tris/HCl, pH 8.5 (UA buffer). Proteins (50 μg) for each sample were reduced by TCEP, alkylated by chloroacetamide, and digested overnight by Lys-C and trypsin (29). Derived peptides were desalted on StageTip C18 (30). Samples were analyzed in duplicate on a LC–ESI–MS-MS quadrupole Orbitrap QExactive-HF Mass Spectrometer (Thermo Fisher Scientific). Peptide separation was achieved on a linear gradient from 95% solvent A (2% ACN, 0.1% formic acid) to 50% solvent B (80% acetonitrile, 0.1% formic acid) over 33 minutes, and from 50% to 100% solvent B in 2 minutes at a constant flow rate of 0.25 μL/min on UHPLC Easy-nLC 1000 (Thermo Fisher Scientific) connected to a 23-cm fused-silica emitter of 75 μm inner diameter (New Objective, Inc.), packed in-house with ReproSil-Pur C18-AQ 1.9 μm beads (Dr Maisch Gmbh) using a high-pressure bomb loader (Proxeon). Mass spectrometry (MS) data were acquired using a data-dependent top 15 method for HCD fragmentation. Survey full-scan MS spectra (300–1650 Th) were acquired in the Orbitrap with 60,000 resolution, AGC target 3e6, IT 20 ms. For HCD spectra, resolution was set to 15,000 at m/z 200, AGC target 1e5, IT 80 ms. For identification and quantitation, Raw MS files were processed with MaxQuant software (1.5.2.8; ref. 31) making use of the Andromeda search engine (32). MS/MS peak lists were searched against the database uniprot_cp_human_2015_03, in which trypsin specificity was used with up to two missed cleavages allowed. Cysteine carbamidomethyl was used as fixed modification, methionine oxidation, and protein N-terminal acetylation as variable modifications. The peptides and protein FDR were set to 0.01; the minimal length required for a peptide was six amino acids; a minimum of two peptides, of which one unique was required for protein identification. Normalized LFQ proteins intensities were analyzed via Perseus (version 1.5.6.0). *T* test statistical analysis was performed applying FDR < 0.05. Cellular component GO and biological pathway analysis was performed via String version 10.5 (https://string-db.org/), using the Gene ID of the identified proteins.

Statistical analysis

Statistical analysis was performed using the GraphPad Prism 5.0 Software (GraphPad Software Inc.). Significance of differences among two or more groups were evaluated by unpaired Student *t* test or one-way ANOVA followed by Bonferroni *post hoc* test. The relation between extracellular vesicle plasma concentrations and matched tumor size was evaluated by correlation analysis. Data are graphed as mean ± 95% confidence intervals (CI). In Kaplan–Meier curves, survival differences were compared by log-rank test. Differences were considered statistically significant when $P < 0.05$.

Results

Human GBMs release multiple extracellular vesicles *in vivo*

GBM cells secrete in culture a heterogeneous population of extracellular vesicles, encompassing exosomes and microvesicles, varying in size from 50 to 1,000 nm (18). By transmission electron microscopy (TEM), we provide evidence that human GBM tissues contain multivesicular bodies (MVB) with exosome-like vesicles inside, with an average diameter of 30–80 nm, and shed microvesicles ranging in size from 100 to 1,000 nm (Fig. 1A–D).

On the basis of previous reports that GBM-derived extracellular vesicles are able to cross the blood–brain barrier and enter the general circulation (4, 11, 14, 17), we isolated by differential centrifugation and characterized extracellular vesicles from plasma of patients with GBM (22). TEM revealed a number of structures of exosomal size and appearance mixed with larger vesicles (Fig. 1E). Thus, in line with our observations on tissues (Fig. 1A–D), GBM-derived extracellular vesicles comprise both exosomes and microvesicles, and express CD9 antigen (Fig. 1F). Moreover, immunoblot analysis revealed the presence of the exosomal protein markers CD9, CD63, and TSG101 in plasma extracellular vesicles from both GBM and control samples (Fig. 1G). Altogether, these results highlight the feasibility to isolate GBM-derived extracellular vesicles from the plasma of patients with GBM.

Circulating extracellular vesicles distinguish patients with GBM from healthy controls

To verify the potential value of circulating extracellular vesicles as a biomarker for GBM, we isolated extracellular vesicles from plasma of patients with GBM at diagnosis (before the operation; baseline) and in parallel from age- and sex-matched healthy controls. Significantly higher numbers of circulating extracellular vesicles were found at baseline in patients with GBM

Downloaded from clincancerres.aacrjournals.org on January 27, 2021. © 2019 American Association for Cancer Research.

Published OnlineFirst October 4, 2018; DOI: 10.1158/1078-0432.CCR-18-1941

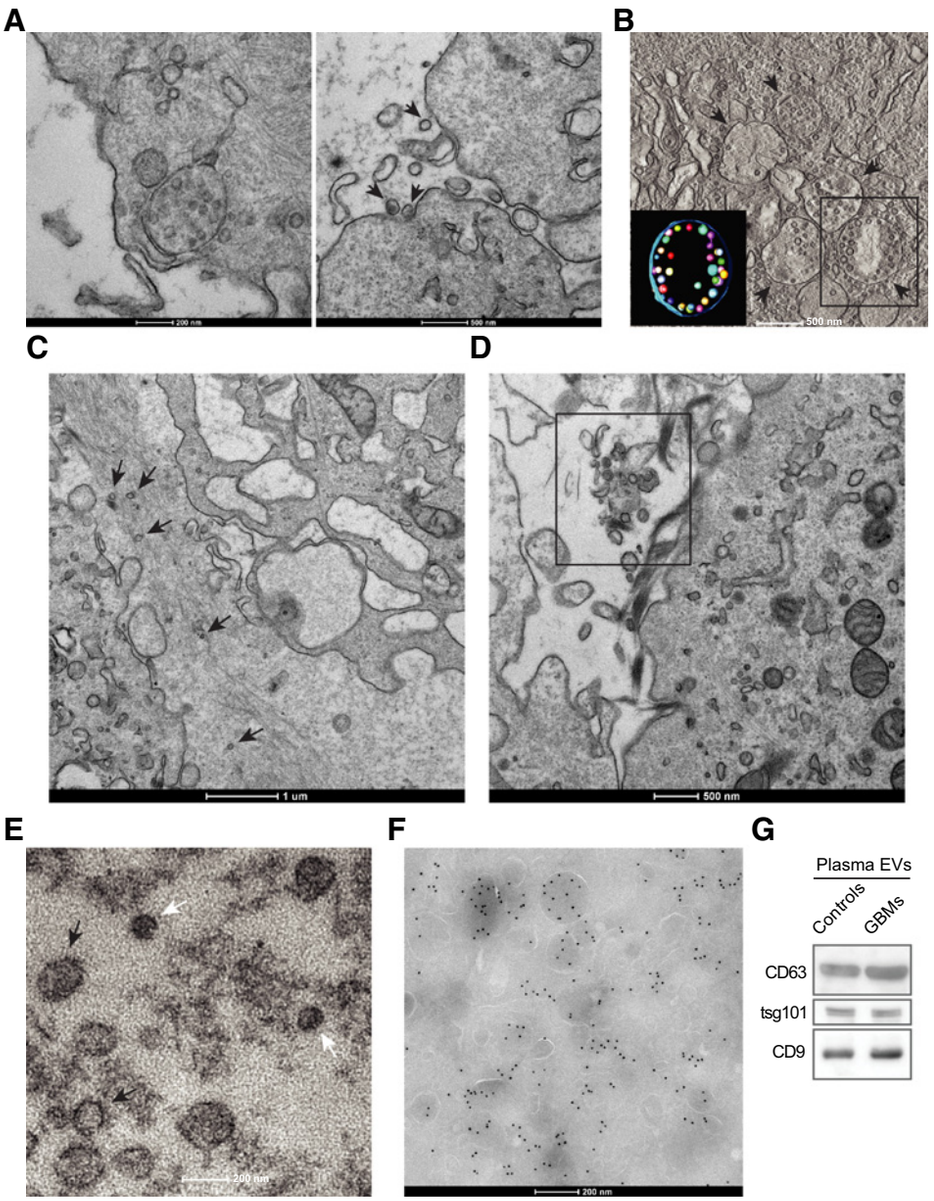

Figure 1.
In vivo release of different EV (extracellular vesicle) types from human GBM tissues. **A,** Representative TEM images of a GBM tissue containing multivesicular bodies (MVB) holding exosome-like intraluminal vesicles (left) and microvesicles (right, black arrows; high magnification, 49,000 ×). **B,** Electron microscope tomography image of a GBM cell containing several MVB (black arrows). The box indicates the area from which the three-dimensional tomographic reconstruction of MVB (black box) was performed. **C,** Appearance of extracellular vesicles (black arrows) in the extracellular space of GBM tissue (magnification 7,800 ×). **D,** Aggregate of extracellular vesicles (boxed area) in the extracellular space of a GBM tissue (magnification 9,600 ×). **E,** A representative TEM image of extracellular vesicles isolated from GBM patient plasma and comprising both exosomes (white arrows) and microvesicles (black arrows; high magnification, 25,000 ×). **F,** GBM patient plasma extracellular vesicles as in (**E**) after immuno-gold labeling with anti-CD9 antibody (high magnification, 29,000 ×). **G,** A representative Western blot analysis showing the expression of the exosomal markers CD9, CD63, and TSG101 in extracellular vesicles derived from GBM and control plasma.

($n = 13$) compared with healthy controls ($n = 17$; discovery patient cohort in Supplementary Table S1), as assessed by NTA ($P < 0.0001$; Fig. 2A). Analysis of an independent patient cohort (validation patient cohort in Supplementary Table S2) confirmed the significant extracellular vesicle enrichment in plasma from patients with GBM ($n = 30$) compared with healthy individuals ($n = 16$; $P = 0.0099$; Fig. 2B). Of note, the average size of GBM- and healthy control–derived extracellular vesicles were similar in discovery ($P = 0.548$) and validation cohort ($P = 0.075$; Fig. 2C and D). Thus, extracellular vesicle concentration, not their size, distinguishes patients with GBM from healthy controls.

The amount of circulating extracellular vesicles was not affected by tumor size ($P = 0.318$, correlation analysis: $r = -0.179$; Supplementary Fig. S1A). However, the extent of necrosis influenced the degree of secretion ($P = 0.045$): higher necrosis in GBM samples (grade III) substantially reduced extracellular vesicle secretion (Supplementary Fig. S1B). No correlation was observed between extracellular vesicle enumeration and the molecular markers routinely tested in clinical practice for GBM, namely EGFR amplification ($P = 0.526$; Supplementary Fig. S1C), phosphatase and tensin homolog (*PTEN*) deletion ($P = 0.761$; Supplementary Fig. S1D), O^6-methylguanine DNA methyltransferase (MGMT) expression ($P = 0.189$; Supplementary Fig. S1E), and isocitrate dehydrogenase 1 and 2 (*IDH1* and *IDH2*) mutations (data not shown). Only GBMs harboring P53 mutations were found to secrete fewer extracellular vesicles ($P = 0.0473$; Supplementary Fig. S1F). Next, we tested for possible associations between plasma extracellular vesicle concentration and patient outcomes. Patients with GBM were ranked according to their extracellular vesicle content and divided into high-content or low-content groups; no significant differences in PFS (log-rank test, $\chi^2 = 0.057$; $P = 0.812$; Supplementary Fig. S1G) or OS (log-rank

Downloaded from clincancerres.aacrjournals.org on January 27, 2021. © 2019 American Association for Cancer Research.

Published OnlineFirst October 4, 2018; DOI: 10.1158/1078-0432.CCR-18-1941

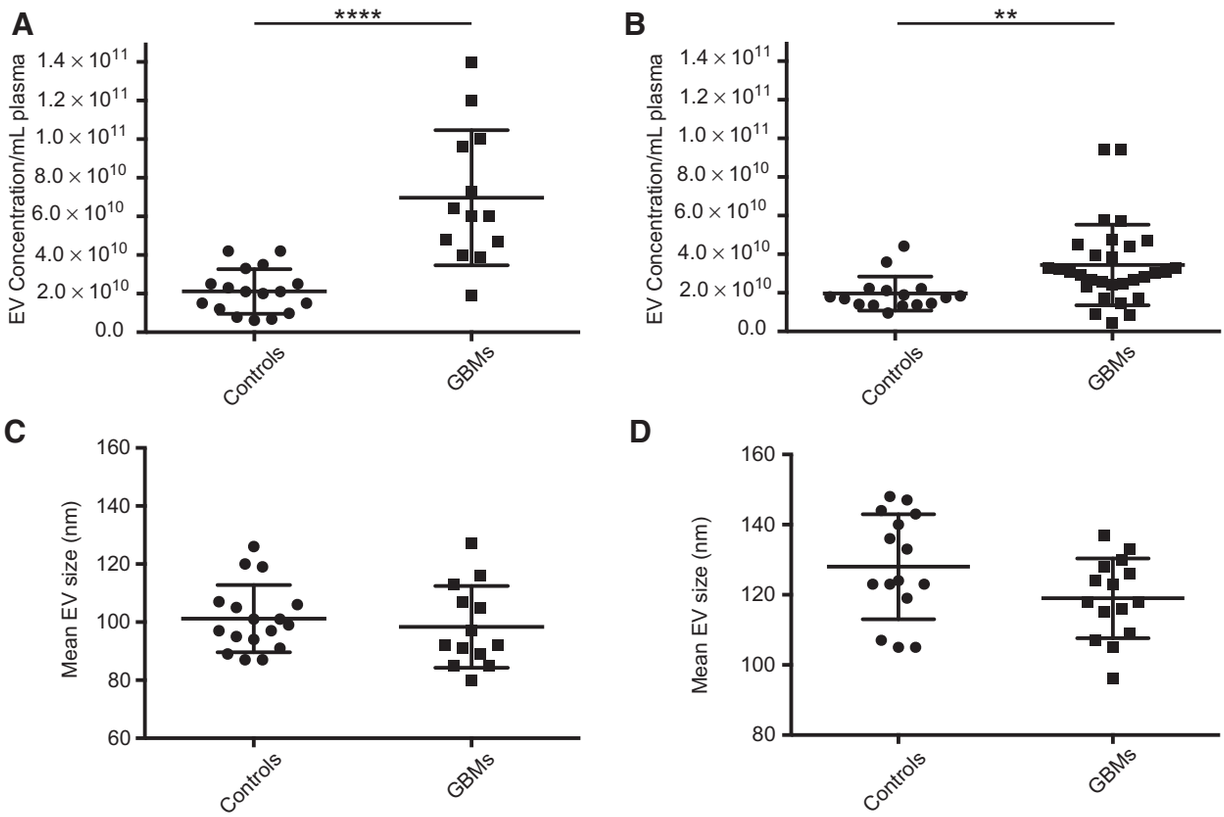

Figure 2.

EV (extracellular vesicle) enrichment in plasma from patients with GBM. **A** and **B,** Extracellular vesicles isolated from plasma of patients with GBM at diagnosis (before surgery) and from age- and sex-matched healthy controls were quantified by NTA. The amount of plasma extracellular vesicles is significantly increased in patients with GBM compared with healthy controls. Left, (discovery cohort: $n = 13$ patients with GBM; $n = 17$ healthy controls): mean extracellular vesicle concentration/mL plasma: 2.12e+10 ± 0.28e+10 95% CI in controls; 6.97e+10 ± 0.97e+10 95% CI in GBMs, $P < 0.0001$; Right, (validation cohort: $n = 30$ patients with GBM; $n = 16$ healthy controls): mean extracellular vesicle concentration/mL plasma: 1.96e+10 ± 0.22e+10 95% CI in controls; 3.45e+10 ± 0.38e+10 95% CI in GBMs, $P = 0.0099$. **C** and **D,** Mean size of GBM- and healthy control-derived extracellular vesicle as in **A** and **B**, assessed by NTA. Left, discovery cohort ($P = 0.548$); right, validation cohort ($P = 0.075$).

test, $\chi^2 = 2.051$; $P = 0.152$; Supplementary Fig. S1H) were found. These results point out that the enumeration of circulating extracellular vesicles in plasma could represent a reliable biomarker for GBM detection independently of tumor subtype or molecular expression.

Extracellular vesicle enrichment is associated with GBM diagnosis

We assessed the specificity of extracellular vesicle enrichment in patients with GBM by collecting plasma samples from other brain lesions which share with GBMs the vascular permeability to gadolinium and other macromolecules. We investigated extracellular vesicle levels in case-control cohorts that included patients with intraaxial lesions (metastases; $n = 13$) and extraaxial brain tumors [adenomas ($n = 3$), meningiomas ($n = 6$), and neurinomas ($n = 3$)]. Interestingly, extracellular vesicle concentrations were similar in healthy controls and in patients with either brain metastases or extraaxial brain tumors: in all groups the extracellular vesicle levels were significantly lower by Bonferroni multiple *t* test than in patients with GBM ($P < 0.0001$; Fig. 3). Overall, these findings suggest that the preoperative plasma extracellular vesicle enrichment is specific for GBM, and plasma extracellular vesicle concentration could be used to distinguish patients with GBM not only from healthy subjects but also from patients with other brain lesions.

Tumor cells are mainly responsible for extracellular vesicle enrichment in GBM patients' plasma

Blood contains a variety of extracellular vesicles released from many different cell types, above all platelets, leukocytes, erythrocytes, and endothelial cells (33). To identify the contribution of GBM-derived extracellular vesicles to the whole circulating extracellular vesicle population, we measured extracellular vesicle concentration in paired pre- and postoperative GBM plasma samples ($n = 14$). The levels of circulating extracellular vesicles were significantly reduced in the postoperative samples ($P = 0.0022$; Fig. 4A), suggesting that they were in part released by GBM cells.

As a confirmation of the tumor origin of extracellular vesicles, we employed the orthotopic transplantation of TICs isolated from human GBM as a model to fully recapitulate GBM pathophysiology (28). By lentiviral transduction, we generated GBM TICs

Downloaded from clincancerres.aacrjournals.org on January 27, 2021. © 2019 American Association for Cancer Research.

Published OnlineFirst October 4, 2018; DOI: 10.1158/1078-0432.CCR-18-1941

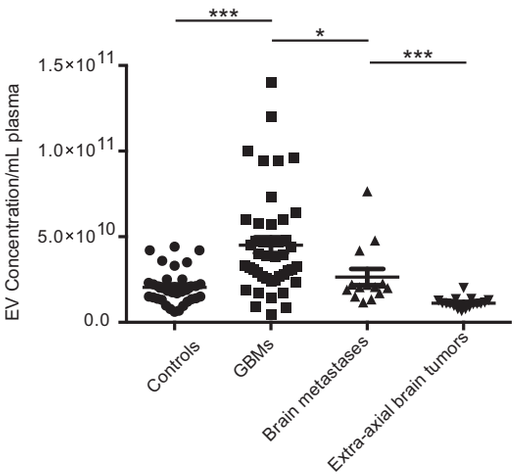

Figure 3.

Specificity of plasma EV (extracellular vesicle) enrichment for patients with GBM. Plasma extracellular vesicle isolated from patients with GBM at diagnosis (before surgery; $n = 43$), patients with brain metastases ($n = 13$) or extra-axial brain tumors ($n = 12$), and healthy controls ($n = 33$) were quantified by NTA ($P < 0.0001$). Patients with GBM had significantly increased plasma extracellular vesicle concentration compared with all the other groups.

expressing the exosomal marker CD9 fused with the GFP protein. Because GBM-derived extracellular vesicles express CD9 on their surface (ref. 34; Fig. 1C), they were identified by tracking the GFP signal, distinct from endogenous GFP-negative murine extracellular vesicles. A homogeneous population of GFP-expressing TICs was isolated by FACS. Representative histograms of control (Supplementary Fig. S2A) and transducedsorted cells (Supplementary Fig. S2B) indicated that almost 20% of the whole cell population was highly GFP-expressing cells (Supplementary Fig. S2B, right). FACS-isolated CD9-GFP$^+$ TICs were orthotopically transplanted into nude mice to generate a GFP$^+$ GBM (Supplementary Fig. S2C). Seven days later, extracellular vesicles were isolated from peripheral blood plasma by differential centrifugation. Extracellular vesicles were significantly enriched in plasma from mice harboring intracranial human GBMs with respect to nontransplanted mice ($P = 0.0322$; Fig. 4B). No difference in plasma extracellular vesicle size was observed between control and GBM-bearing mice: the average size of extracellular vesicles was 117 $\pm$ 5.43 nm versus 120.2 $\pm$ 5.00 nm in control and tumor-bearing mice, respectively ($P = 0.68$). Once isolated, murine plasma extracellular vesicles were stained with DiI and analyzed by CLSM for CD9-GFP and DiI. GFP-specific signal was detected in plasma extracellular vesicles derived from GBM-transplanted mice, while being undetectable in nontransplanted mouse plasma extracellular vesicles (Fig. 4C). Extracellular vesicles (35%) detectable by CLSM were DiI$^+$GFP$^+$, 49% were DiI$^+$GFP$^-$, and 16% DiI$^-$GFP$^+$

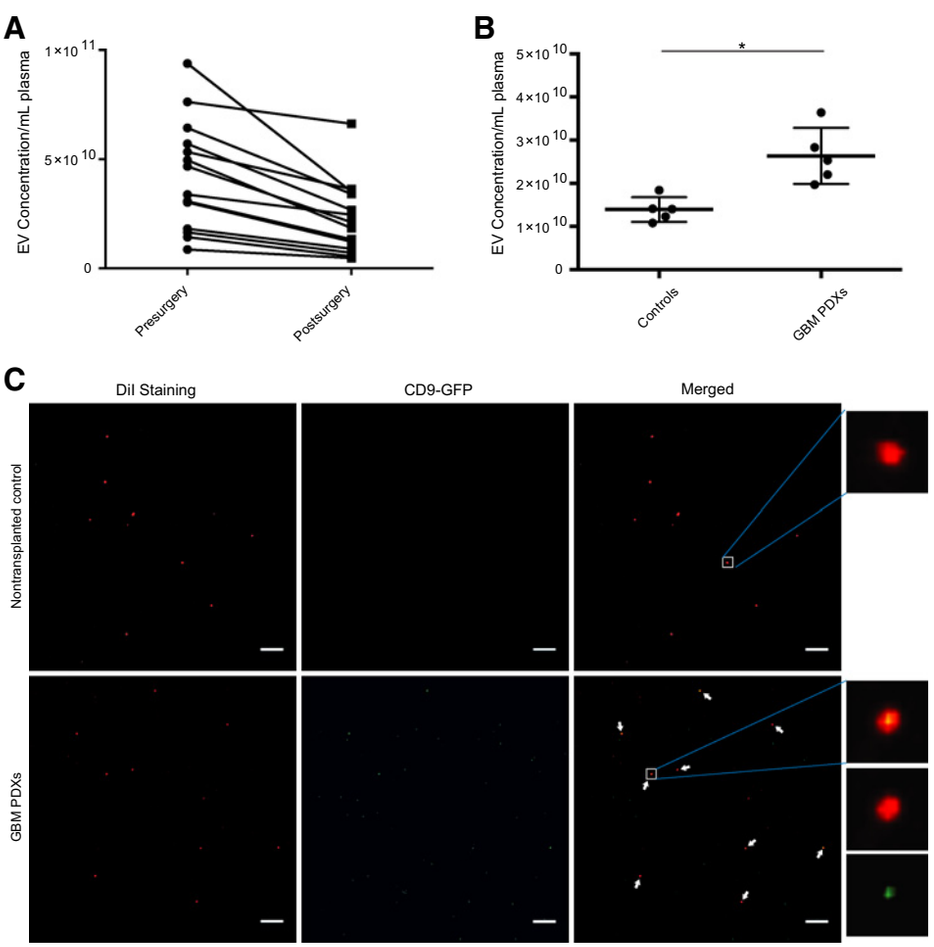

Figure 4.

Association between EV (extracellular vesicle) enrichment in GBM patients' plasma and tumor. **A,** Extracellular vesicle concentrations in paired pre- and postoperative plasma samples from GBMs ($n = 14$) were quantified by NTA ($P = 0.0022$). **B,** Extracellular vesicle concentrations in plasma from nontransplanted mice or mice harboring intracranial human GBMs (GBM PDXs) were quantified by NTA (mean extracellular vesicle concentration/mL plasma: 1.498e+10 $\pm$ 0.413e+10 95% CI in controls; 3.028e+10 $\pm$ 0.392e+10 95% CI in GBM PDXs, $P = 0.0322$; n = 5 mice/group). **C,** Plasma extracellular vesicles from nontransplanted mice or mice harboring intracranial human GBMs were stained with the membrane dye DiI and analyzed by CLSM. Representative images of DiI$^+$ (red) and GFP$^+$ (green) extracellular vesicle are shown. Scale bar = 12 μm. Insets on the right show higher magnification.

Downloaded from clincancerres.aacrjournals.org on January 27, 2021. © 2019 American Association for Cancer Research.

Published OnlineFirst October 4, 2018; DOI: 10.1158/1078-0432.CCR-18-1941

only, confirming previous observations that DiI does not stain all extracellular vesicles (35). Taken together, these findings indicated that nearly half of extracellular vesicles in the peripheral circulation of transplanted mice were tumor-derived ($DiI^{+}GFP^{+}$ or $DiI^{-}GFP^{+}$). Combined with the significant decrease in circulating extracellular vesicles after GBM removal, these data suggest that the direct release by GBM tumor mass significantly contributed to the increased circulating extracellular vesicle levels in patients with GBM.

The level of circulating extracellular vesicles informs on GBM relapse

To understand whether circulating extracellular vesicles could inform on therapeutic interventions and anticipate tumor recurrence, we compared plasma extracellular vesicle concentrations from patients facing a relapse ($n = 9$) with extracellular vesicle concentrations from either preoperative GBM plasma samples or the matched postoperative GBM samples ($n = 14$). Plasma extracellular vesicles are enriched in preoperative GBM plasma samples, significantly decline after the resection of the primary GBMs, and raise again when the tumor relapses ($P = 0.028$; Fig. 5): the level of extracellular vesicles in recurrent GBMs was nearly 40% higher than in the primary GBM samples at the immediate postresection assessment, being higher than the extracellular vesicle level in healthy controls (Fig. 2A and B). Combined with the significant decrease in circulating extracellular vesicles after GBM removal, extracellular vesicle enrichment at relapse suggests a direct link between extracellular vesicles and the presence of a GBM mass.

GBM extracellular vesicle protein cargo provides a set of known glioma targets

We compared with MS the protein cargo of plasma extracellular vesicles from pools of patients with GBM and of healthy controls. We normalized GBM and healthy control samples for extracellular vesicle concentration. The pattern obtained after Coomassie staining of extracellular vesicle lysates revealed the absence of striking differences in the proteomic profiles of extracellular vesicles from GBM plasma samples versus controls (Supplementary Fig. S3A). Significant and differentially expressed proteins were selected by performing a *t* test analysis, using $P < 0.05$ and FDR < 0.05 as cutoff. The first MS analysis identified 406 differentially expressed proteins (SET1, Supplementary Table S3). Almost all the proteins identified had been already annotated as extracellular vesicle components (GO cellular component SET1; Supplementary Table S3) and included ribosomal proteins, annexins, integrins, heat shock proteins, G proteins and Ras-related, tetraspanins, histones, and proteins involved in exosome biogenesis. Of these, 123 proteins were specifically enriched in GBMs, while 257 were specifically enriched in controls (Fig. 6A; Supplementary Table S4). To verify the robustness of these proteomic identifications, a second MS analysis was performed on extracellular vesicles purified from a new pool of plasma from patients with GBM, resulting in the identification of 245 proteins (SET2, Supplementary Table S3); almost all of these proteins were annotated as extracellular vesicle components (GO cellular component SET2, Supplementary Table S3). Of these, 44 proteins were specifically enriched in GBMs, while 48 were specifically enriched in controls (Fig. 6B; Supplementary Table S3). Taking into account that we pooled plasma extracellular vesicles derived from different patients with GBM and healthy controls, the heterogeneity among the two analyses is not surprising. GBM extracellular vesicles derived from the two experiments shared 19 common upregulated proteins (Fig. 6C; Supplementary Table S4). Pathway analysis revealed enrichment in inflammation and immune response, growth, survival, and migration, as well as metabolic-regulated proteins (Pathway enrichment GBM SET1–SET2, Supplementary Table S4). To study how the extracellular vesicle proteome is influenced by the GBM mass, we profiled the protein cargo of plasma extracellular vesicles derived from matched GBM patients before and after surgery and found 102 differentially expressed proteins (Fig. 6D and pathway enrichment PRE_POST Supplementary Table S4). Finally, from the comparison of the three GBM extracellular vesicle sets, we identified 11 common proteins (vWF, APCS, C4B, AMBP, APOD, AZGP1, C4BPB, Serpin3, FTL, C3, and APOE), known to be members of the complement and coagulation cascade and regulators of iron metabolism, and defining what we call "the GBM EV protein signature" (Fig. 6E). Interestingly, that signature disappeared after GBM surgery (Supplementary Table S4), reflecting tumor-dependent expression patterns essential to maintain tumors and allowing the distinction of patients with GBM from healthy controls. The subsequent validation of this signature in The Cancer Genome Atlas GBM dataset, which comprises 543 patients (http://cancergenome.nih.gov/), revealed the overexpression of some members (FTL, vWF, AZGP1, Serpin 3, C3, and APOE) in GBMs compared with nonneoplastic brains (Supplementary Fig. S3B), thus suggesting their potential involvement in GBM pathophysiology.

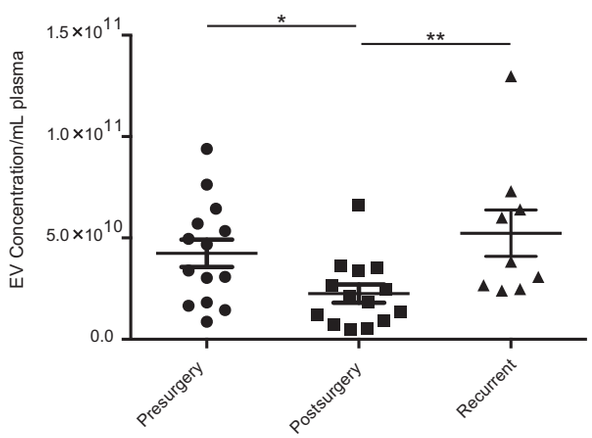

Figure 5.

Association between level of circulating EVs (extracellular vesicles) and the GBM. Extracellular vesicles concentrations in matched pre- and postoperative GBM samples ($n = 14$) and in patients facing a relapse ($n = 9$) were assessed by NTA ($P = 0.028$). Plasma extracellular vesicles are enriched in preoperative GBM plasma samples, significantly decline after GBM removal in the matched postoperative samples, and rise again when the tumor relapses.

Discussion

We report herein an increased concentration of plasma extracellular vesicles in patients with GBM compared with healthy controls. The extracellular vesicle increment disappeared after surgical removal, returning to a level comparable with that of healthy controls. Interestingly, at recurrence, an increase in plasma extracellular vesicles was observed again. We proved the

Downloaded from clincancerres.aacrjournals.org on January 27, 2021. © 2019 American Association for Cancer Research.

Published OnlineFirst October 4, 2018; DOI: 10.1158/1078-0432.CCR-18-1941

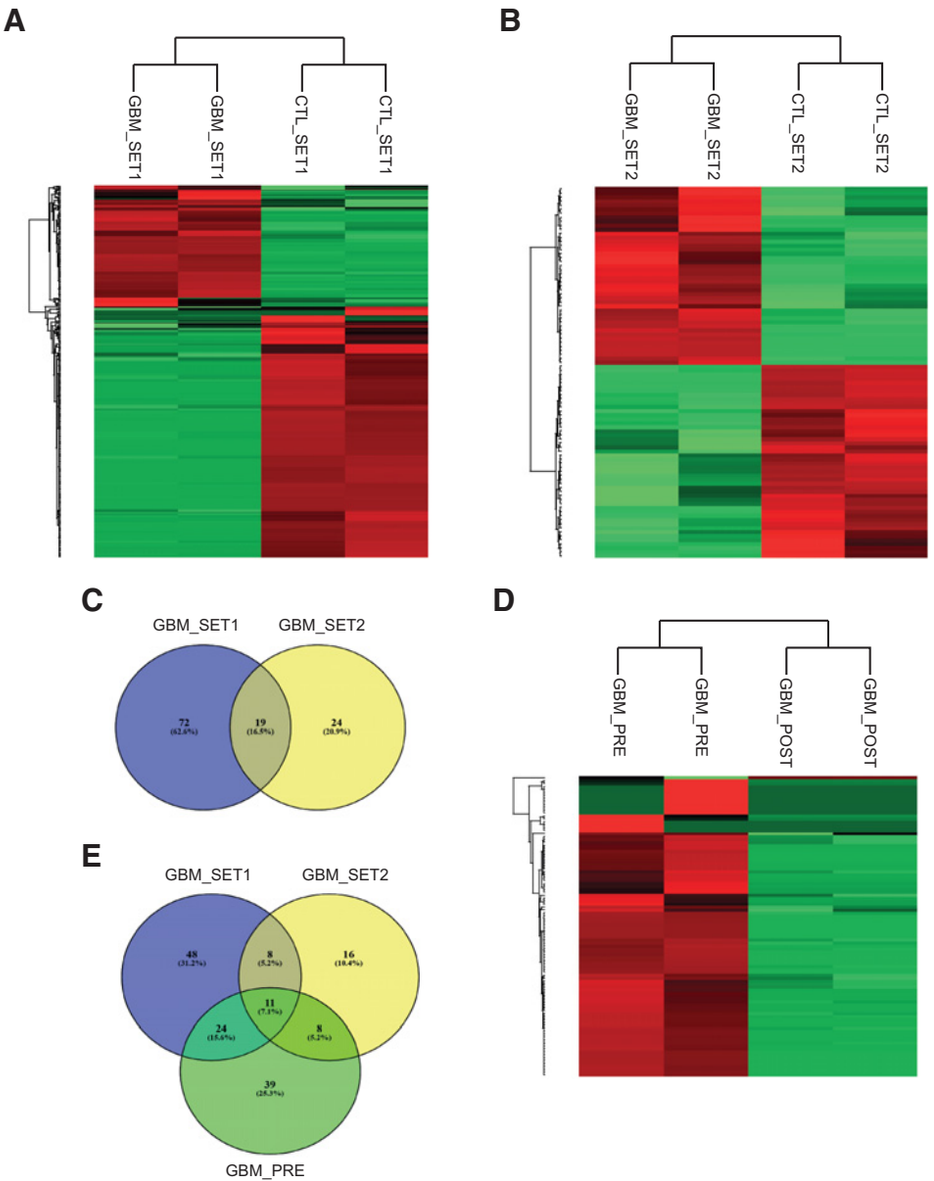

Figure 6.
GBM extracellular vesicle protein cargo definition. **A** and **B,** Heatmap of differentially expressed proteins ($P < 0.05$ and FDR < 0.05) between extracellular vesicles from GBM and control plasma. Two different extracellular vesicles pools from either patients with GBM and healthy controls were analyzed (GBM_SET1 and CTL_SET1; GBM_SET2 and CTL_SET2). **C,** Venn diagram depicting the number of proteins identified by MS in GBM_SET1 and GBM_SET2 analyzed in A and B. **D,** Heatmap displaying significant and differentially expressed proteins ($P < 0.05$ and FDR< 0.05) between extracellular vesicle from paired pre- and postoperative GBM plasma samples (GBM_PRE and GBM_POST). **E,** Venn diagram representing the overlap in statistically significant proteins enriched in the three GBM extracellular vesicle sets.

specificity of this phenomenon by quantifying plasma extracellular vesicles in brain metastases and extra-axial tumors and employing a murine model of GBM (PDX). Plasma extracellular vesicle levels at recurrence were slightly increased in comparison with primary GBM, but did not reach statistical significance. This is in agreement with other preclinical reports (36, 37), showing an effect of treatment, chemo-, and radiotherapy on extracellular vesicle release. In general, our results outline an intriguing phenomenon: the specific ability of GBM to increase the global concentration of plasma extracellular vesicles. This could be the basis to employ plasma extracellular vesicles as a biomarker capable to describe the status of the tumor through a minimally invasive blood sample, as demonstrated by the specific reincrease in concentration at recurrence. This aspect is of particular interest if we consider MRI limitations in correctly distinguishing GBM from brain metastases or other brain lesions (38). Of further interest, our results from the GBM PDX model suggest that the elevated extracellular vesicle levels are informative also in determining the early progression of the tumor. The current available literature instead confers a clinical value to extracellular vesicles in human GBM by virtue of their content, which includes proteins, coding (i.e., EGFRvIII and IDH1 mRNA) and noncoding RNAs (i.e., mir21), and DNA. As such, our work highlights the clinical value of extracellular vesicle enumeration, rather than extracellular vesicle cargo, which demonstrates tumor presence, reflects responses to therapy, and help in following GBM progression. We failed to find a correlation with preoperative MRI and commonly employed molecular markers. We only measured a reduced extracellular vesicle secretion in GBM samples harboring P53 mutations, which fits well with the current literature pointing at P53, the most common altered gene in human cancer cells, as a regulator of exosome release (39–41). Moreover, we found that GBM samples with a higher necrosis release less extracellular vesicles when compared with those GBM tissues with reduced

Downloaded from clincancerres.aacrjournals.org on January 27, 2021. © 2019 American Association for Cancer Research.

Published OnlineFirst October 4, 2018; DOI: 10.1158/1078-0432.CCR-18-1941

necrosis content. This is in line with the general knowledge that viable tissues efficiently release extracellular vesicles in the form of exosomes and MVs. The lack of any correlation between extracellular vesicle concentrations and patient outcome is probably either due to tumor-intrinsic properties (cell composition, proliferation, metabolism, cellular communication, and differentially activated signaling pathways) or to extra-tumor factors, such as tumor location or the clinical status *in toto*, both of them influencing therapeutic response and the outcome itself. In addition, the extreme heterogeneity of GBM poses a great challenge in establishing any association. The bulk of tumor is constituted by different subpopulations of cells: stem, progenitor, and differentiated cells, each with specific molecular features (42). Plasma extracellular vesicle concentrations results from their release from all the viable cells in the tumor. Being the expression of molecular markers highly variable in different cells inside the tumor, the global rate of extracellular vesicle release does not seem affected by specific marker expression. Another possible explanation regards the secretion rate by different subpopulations of GBM cells. It is possible to speculate that the global concentration in plasma is consequence of nonhomogeneous release of extracellular vesicles by different subpopulations, thus making the global concentration not related to markers or tumor/necrosis size (43–45).

In the second part of our work, we characterized the protein cargo of plasma extracellular vesicles in patients with GBM and healthy controls through a MS-based proteomic analysis to identify differentially expressed extracellular vesicle-associated proteins as potential biomarkers. The main differentially expressed protein domains in GBM plasma extracellular vesicles include members of complement and coagulation cascade and regulators of iron metabolism. The role of these proteins has been already described in GBM biology, thus making these targets extremely interesting for extracellular vesicle-based biomarker development (46–53). We demonstrate that the clinical correlation of plasma extracellular vesicles is with the presence of the tumor. Furthermore, the protein cargo is influenced by GBM status in a specific way.

In future studies plasma extracellular vesicle level and protein cargo should be assessed through closer quantifications during patient follow-up to find correlations with MRI, treatment, molecular, and clinical features.

Our preliminary experience sheds light on application of extracellular vesicles as clinical biomarker for patients with GBM. Actually, GBM treatment has to face the impossibility to early detect the recurrence/presence and to timely follow the progression, in the absence of any reliable biomarker. Our findings indicate that the concentration of plasma extracellular vesicles together with the possibility to characterize their specific cargo can be of assistance to the diagnosis and treatment follow-up of patients with GBM.

Disclosure of Potential Conflicts of Interest

No potential conflicts of interest were disclosed.

Authors' Contributions

Conception and design: D. Osti, M. Del Bene, G. Rappa, F. DiMeco, A. Lorico
Development of methodology: D. Osti, M. Del Bene, M. Santos, G.V. Beznoussenko, A. Mironov, A. Bachi, F. DiMeco, A. Lorico, G. Pelicci
Acquisition of data (provided animals, acquired and managed patients, provided facilities, etc.): D. Osti, M. Del Bene, M. Santos, V. Matafora, C. Richichi, S. Faletti, G.V. Beznoussenko, A. Mironov, D. Bongetta, P. Gaetani, F. DiMeco, A. Lorico, G. Pelicci
Analysis and interpretation of data (e.g., statistical analysis, biostatistics, computational analysis): D. Osti, M. Del Bene, G. Rappa, M. Santos, V. Matafora, G.V. Beznoussenko, A. Mironov, A. Bachi, L. Fornasari, P. Gaetani, F. DiMeco, A. Lorico, G. Pelicci
Writing, review, and/or revision of the manuscript: D. Osti, M. Del Bene, G. Rappa, G.V. Beznoussenko, A. Mironov, A. Bachi, F. DiMeco, A. Lorico, G. Pelicci
Administrative, technical, or material support (i.e., reporting or organizing data, constructing databases): D. Osti, M. Del Bene, D. Bongetta
Study supervision: F. DiMeco, A. Lorico

Acknowledgments

We thank Fabio Anzanello for assistance with the nanoparticle tracking analysis, Micaela Quarto for IHC analyses, and the European Centre for Nanomedicine (CEN Foundation, Italy) for the use of Tecnai 20 electron microscope. This work was supported by the Italian Association for Cancer Research Investigator Grant (project code 14069, to G. Pelicci), Fondazione Umberto Veronesi (FUV, to C. Richichi).

The costs of publication of this article were defrayed in part by the payment of page charges. This article must therefore be hereby marked *advertisement* in accordance with 18 U.S.C. Section 1734 solely to indicate this fact.

Received June 21, 2018; revised August 26, 2018; accepted October 1, 2018; published first October 4, 2018.

References

1. Johnson DR, O'Neill BP. Glioblastoma survival in the United States before and during the temozolomide era. J Neurooncol 2012;107:359–64.
2. Stupp R, Mason WP, van den Bent MJ, Weller M, Fisher B, Taphoorn MJB, et al. Radiotherapy plus concomitant and adjuvant temozolomide for glioblastoma. N Engl J Med 2005;352:987–96.
3. Evans SM, Putt M, Yang XY, Lustig RA, Martinez-Lage M, Williams D, et al. Initial evidence that blood-borne microvesicles are biomarkers for recurrence and survival in newly diagnosed glioblastoma patients. J Neurooncol 2016;127:391–400.
4. Mahmoudi K, Ezrin A, Hadjipanayis C. Small extracellular vesicles as tumor biomarkers for glioblastoma. Mol Aspects Med 2015;45:97–102.
5. Valadi H, Ekstrom K, Bossios A, Sjostrand M, Lee JJ, Lotvall JO. Exosome-mediated transfer of mRNAs and microRNAs is a novel mechanism of genetic exchange between cells. Nat Cell Biol 2007;9:654–9.
6. Baulch JE, Geidzinski E, Tran KK, Yu L, Zhou YH, Limoli CL. Irradiation of primary human gliomas triggers dynamic and aggressive survival responses involving microvesicle signaling. Environ Mol Mutagen 2016; 57:405–15.
7. Bronisz A, Godlewski J, Chiocca EA. Extracellular vesicles and microRNAs: their role in tumorigenicity and therapy for brain tumors. Cell Mol Neurobiol 2016;36:361–76.
8. D'Asti E, Chennakrishnaiah S, Lee TH, Rak J. Extracellular vesicles in brain tumor progression. Cell Mol Neurobiol 2016;36:383–407.
9. Gourlay J, Morokoff AP, Luwor RB, Zhu HJ, Kaye AH, Stylli SS. The emergent role of exosomes in glioma. J Clin Neurosci 2017;35:13–23.
10. Mallawaaratchy DM, Hallal S, Russell B, Ly L, Ebrahimkhani S, Wei H, et al. Comprehensive proteome profiling of glioblastoma-derived extracellular vesicles identifies markers for more aggressive disease. J Neurooncol 2017;131:233–44.
11. Nakano I, Garnier D, Minata M, Rak J. Extracellular vesicles in the biology of brain tumor stem cells–implications for inter-cellular communication, therapy and biomarker development. Semin Cell Develop Biol 2015;40:17–26.
12. Quezada C, Torres A, Niechi I, Uribe D, Contreras-Duarte S, Toledo F, et al. Role of extracellular vesicles in glioma progression. Mol Aspects Med 2018;60:38–51.

Downloaded from clincancerres.aacrjournals.org on January 27, 2021. © 2019 American Association for Cancer Research.

Published OnlineFirst October 4, 2018; DOI: 10.1158/1078-0432.CCR-18-1941

13. Barile L, Vassalli G. Exosomes: therapy delivery tools and biomarkers of diseases. Pharmacol Thera 2017;174:63–78.
14. Soung YH, Ford S, Zhang V, Chung J. Exosomes in cancer diagnostics. Cancers 2017;9:8.
15. Melo SA, Luecke LB, Kahlert C, Fernandez AF, Gammon ST, Kaye J, et al. Glypican-1 identifies cancer exosomes and detects early pancreatic cancer. Nature 2015;523:177.
16. Al-Nedawi K, Meehan B, Micallef J, Lhotak V, May L, Guha A, et al. Intercellular transfer of the oncogenic receptor EGFRvIII by microvesicles derived from tumour cells. Nat Cell Biol 2008;10:619–24.
17. Shao H, Chung J, Balaj L, Charest A, Bigner DD, Carter BS, et al. Protein typing of circulating microvesicles allows real-time monitoring of glioblastoma therapy. Nat Med 2012;18:1835–40.
18. Skog J, Wurdinger T, van Rijn S, Meijer DH, Gainche L, Sena-Esteves M, et al. Glioblastoma microvesicles transport RNA and proteins that promote tumour growth and provide diagnostic biomarkers. Nat Cell Biol 2008;10:1470–6.
19. Joo KM, Kim J, Jin J, Kim M, Seol HJ, Muradov J, et al. Patient-specific orthotopic glioblastoma xenograft models recapitulate the histopathology and biology of human glioblastomas *in situ*. Cell Rep 2013;3:260–73.
20. Takami H, Yoshida A, Fukushima S, Arita H, Matsushita Y, Nakamura T, et al. Revisiting TP53 mutations and immunohistochemistry–a comparative study in 157 diffuse gliomas. Brain Pathol 2015;25:256–65.
21. Wen PY, Macdonald DR, Reardon DA, Cloughesy TF, Sorensen AG, Galanis E, et al. Updated response assessment criteria for high-grade gliomas: response assessment in neuro-oncology working group. J Clin Oncol 2010;28:1963–72.
22. Thery C, Amigorena S, Raposo G, Clayton A. Isolation and characterization of exosomes from cell culture supernatants and biological fluids. Curr Protoc Cell Biol 2006;Chapter 3:Unit 3.22.
23. Kolpakov V, Polishchuk R, Bannykh S, Rekhter M, Solovjev P, Romanov Y, et al. Atherosclerosis-prone branch regions in human aorta: microarchitecture and cell composition of intima. Atherosclerosis 1996;122:173–89.
24. Mironov AA, Colanzi A, Polishchuk RS, Beznoussenko GV, Mironov AA Jr, Fusella A, et al. Dicumarol, an inhibitor of ADP-ribosylation of CtBP3/BARS, fragments golgi non-compact tubular zones and inhibits intra-golgi transport. Eur J Cell Biol 2004;83:263–79.
25. Setti M, Osti D, Richichi C, Ortensi B, Del Bene M, Fornasari L, et al. Extracellular vesicle-mediated transfer of CLIC1 protein is a novel mechanism for the regulation of glioblastoma growth. Oncotarget 2015;6:31413–27.
26. Beznoussenko GV, Mironov AA. Correlative video-light-electron microscopy of mobile organelles. Methods Mol Biol 2015;1270:321–46.
27. Rappa G, Mercapide J, Anzanello F, Pope RM, Lorico A. Biochemical and biological characterization of exosomes containing prominin-1/CD133. Mol Cancer 2013;12:62.
28. Richichi C, Osti D, Del Bene M, Fornasari L, Patane M, Pollo B, et al. Tumor-initiating cell frequency is relevant for glioblastoma aggressiveness. Oncotarget 2016;7:71491–503.
29. Kulak NA, Pichler G, Paron I, Nagaraj N, Mann M. Minimal, encapsulated proteomic-sample processing applied to copy-number estimation in eukaryotic cells. Nat Methods 2014;11:319–24.
30. Rappsilber J, Ishihama Y, Mann M. Stop and go extraction tips for matrix-assisted laser desorption/ionization, nanoelectrospray, and LC/MS sample pretreatment in proteomics. Anal Chem 2003;75:663–70.
31. Cox J, Mann M. MaxQuant enables high peptide identification rates, individualized p.p.b.-range mass accuracies and proteome-wide protein quantification. Nat Biotechnol 2008;26:1367–72.
32. Cox J, Neuhauser N, Michalski A, Scheltema RA, Olsen JV, Mann M. Andromeda: a peptide search engine integrated into the MaxQuant environment. J Proteome Res 2011;10:1794–805.
33. de Vooght KM, Lau C, de Laat PP, van Wijk R, van Solinge WW, Schiffelers RM. Extracellular vesicles in the circulation: are erythrocyte microvesicles a confounder in the plasma haemoglobin assay? Biochem Soc Trans 2013;41:288–92.
34. Galbo PM, Ciesielski MJ, Figel S, Maguire O, Qiu J, Wiltsie L, et al. Circulating CD9+/GFAP+/survivin+ exosomes in malignant glioma patients following survivin vaccination. Oncotarget 2017;8:114722–35.
35. Rappa G, Santos MF, Green TM, Karbanova J, Hassler J, Bai Y, et al. Nuclear transport of cancer extracellular vesicle-derived biomaterials through nuclear envelope invagination-associated late endosomes. Oncotarget 2017;8:14443–61.
36. Andre-Gregoire G, Bidere N, Gavard J. Temozolomide affects extracellular vesicles released by glioblastoma cells. Biochimie 2018.
37. Arscott WT, Tandle AT, Zhao S, Shabason JE, Gordon IK, Schlaff CD, et al. Ionizing radiation and glioblastoma exosomes: implications in tumor biology and cell migration. Translat Oncol 2013;6:638–48.
38. Weber MA, Zoubaa S, Schlieter M, Jüttler E, Huttner HB, Geletneky K, et al. Diagnostic performance of spectroscopic and perfusion MRI for distinction of brain tumors. Neurology 2006;66:1899.
39. Sun Y, Zheng W, Guo Z, Ju Q, Zhu L, Gao J, et al. A novel TP53 pathway influences the HGS-mediated exosome formation in colorectal cancer. Sci Rep 2016;6:28083.
40. Yu X, Harris SL, Levine AJ. The regulation of exosome secretion: a novel function of the p53 protein. Cancer Res 2006;66:4795–801.
41. Yu X, Riley T, Levine AJ. The regulation of the endosomal compartment by p53 the tumor suppressor gene. FEBS J 2009;276:2201–12.
42. Patel AP, Tirosh I, Trombetta JJ, Shalek AK, Gillespie SM, Wakimoto H, et al. Single-cell RNA-seq highlights intratumoral heterogeneity in primary glioblastoma. Science 2014;344:1396–401.
43. Ellingson BM, Abrey LE, Nelson SJ, Kaufmann TJ, Garcia J, Chinot O, et al. Validation of postoperative residual contrast enhancing tumor volume as an independent prognostic factor for overall survival in newly diagnosed glioblastoma. Neuro Oncol 2018;20:1240–50.
44. Filippini G, Falcone C, Boiardi A, Broggi G, Bruzzone MG, Caldiroli D, et al. Prognostic factors for survival in 676 consecutive patients with newly diagnosed primary glioblastoma. Neuro Oncol 2008;10:79–87.
45. Jeremic B, Milicic B, Grujicic D, Dagovic A, Aleksandrovic J, Nikolic N. Clinical prognostic factors in patients with malignant glioma treated with combined modality approach. Am J Clin Oncol 2004;27:195–204.
46. Bouwens TAM, Trouw LA, Veerhuis R, Dirven CMF, Lamfers MLM, Al-Khawaja H. Complement activation in Glioblastoma Multiforme pathophysiology: Evidence from serum levels and presence of complement activation products in tumor tissue. J Neuroimmunol 2015;278:271–6.
47. Gollapalli K, Ray S, Srivastava R, Renu D, Singh P, Dhali S, et al. Investigation of serum proteome alterations in human glioblastoma multiforme. Proteomics 2012;12:2378–90.
48. Hunter SB, Varma V, Shehata B, Nolen JD, Cohen C, Olson JJ, et al. Apolipoprotein D expression in primary brain tumors: analysis by quantitative RT-PCR in formalin-fixed, paraffin-embedded tissue. J Histochem Cytochem 2005;53:963–9.
49. Luo D, Chen W, Tian Y, Li J, Xu X, Chen C, et al. Serpin peptidase inhibitor, clade A member 3 (SERPINA3), is overexpressed in glioma and associated with poor prognosis in glioma patients. OncoTargets Ther 2017;10:2173–81.
50. Nicoll JA, Zunarelli E, Rampling R, Murray LS, Papanastassiou V, Stewart J. Involvement of apolipoprotein E in glioblastoma: immunohistochemistry and clinical outcome. Neuroreport 2003;14:1923–6.
51. Nowacki P, Tabaka J. Human von Willebrand factor (factor VIII-related antigen) in glial neoplastic cells of brain gliomas. Folia Neuropathol 2003;41:23–7.
52. Park YE, Yeom J, Kim Y, Lee HJ, Han KC, Lee ST, et al. Identification of plasma membrane glycoproteins specific to human glioblastoma multiforme cells using lectin arrays and LC-MS/MS. Proteomics 2018;18.
53. Wu T, Li Y, Liu B, Zhang S, Wu L, Zhu X, et al. Expression of ferritin light chain (FTL) is elevated in glioblastoma, and FTL silencing inhibits glioblastoma cell proliferation via the GADD45/JNK pathway. PLoS One 2016;11:e0149361.

Downloaded from clincancerres.aacrjournals.org on January 27, 2021. © 2019 American Association for Cancer Research.

Published OnlineFirst October 4, 2018; DOI: 10.1158/1078-0432.CCR-18-1941

AACR American Association for Cancer Research

Clinical Cancer Research

Clinical Significance of Extracellular Vesicles in Plasma from Glioblastoma Patients

Daniela Osti, Massimiliano Del Bene, Germana Rappa, et al.

Clin Cancer Res 2019;25:266-276. Published OnlineFirst October 4, 2018.

Updated version Access the most recent version of this article at: doi:10.1158/1078-0432.CCR-18-1941

Supplementary Material Access the most recent supplemental material at: http://clincancerres.aacrjournals.org/content/suppl/2018/10/04/1078-0432.CCR-18-1941.DC1 http://clincancerres.aacrjournals.org/content/suppl/2020/01/30/1078-0432.CCR-18-1941.DC2

Cited articles This article cites 50 articles, 4 of which you can access for free at: http://clincancerres.aacrjournals.org/content/25/1/266.full#ref-list-1

Citing articles This article has been cited by 1 HighWire-hosted articles. Access the articles at: http://clincancerres.aacrjournals.org/content/25/1/266.full#related-urls

E-mail alerts Sign up to receive free email-alerts related to this article or journal.

Reprints and Subscriptions To order reprints of this article or to subscribe to the journal, contact the AACR Publications Department at pubs@aacr.org.

Permissions To request permission to re-use all or part of this article, use this link http://clincancerres.aacrjournals.org/content/25/1/266. Click on "Request Permissions" which will take you to the Copyright Clearance Center's (CCC) Rightslink site.

Downloaded from clincancerres.aacrjournals.org on January 27, 2021. © 2019 American Association for Cancer Research.